Biogeosciences Discuss., 8, 3009–3050, 2011
www.biogeosciences-discuss.net/8/3009/2011/
doi:10.5194/bgd-8-3009-2011

Biogeosciences Discussions

Inferring phytoplankton carbon and eco-physiological rates from diel cycles of spectral particulate beam-attenuation coefficient

G. Dall'Olmo[1], T. K. Westberry[2], M. J. Behrenfeld[2], E. Boss[3], C. Courties[4,5], L. Prieur[6,7], N. Hardman-Mountford[1], and T. Moutin[8]

[1]Plymouth Marine Laboratory, Prospect Place, The Hoe, Plymouth, PL1 3DH, UK
[2]Department of Botany and Plant Pathology, Oregon State University, Corvallis, OR, 97331, USA
[3]MISC Lab, University of Maine, 458 Aubert Hall, Orono, ME 04469, USA
[4]CNRS, UMS 2348, Observatoire Océanologique, 66650 Banyuls sur mer, France
[5]UPMC Univ Paris 06, UMS 2348, Observatoire Océanologique, 66650 Banyuls sur mer, France
[6]CNRS, UMR 7093, Laboratoire d'Océanographie de Villefranche, Observatoire Océanologique, 06234 Villefranche/mer, France

[7]UPMC Univ Paris 06, UMR 7093, Laboratoire d'Océanographie de Villefranche, Observatoire Océanologique, 06230 Villefranche/mer, France
[8]INSU-CNRS, Laboratoire d'Océanographie Physique et Biogéochimique, UMR 6535, Centre d'Océanologie de Marseille, Université de la Mediterranée, France

Received: 15 March 2011 – Accepted: 15 March 2011 – Published: 21 March 2011

Correspondence to: G. Dall'Olmo (gdal@pml.ac.uk)

Published by Copernicus Publications on behalf of the European Geosciences Union.

Abstract

The diurnal fluctuations in solar irradiance impose a fundamental frequency on ocean biogeochemistry. Observations of the ocean carbon cycle at these frequencies are rare, but could be considerably expanded by measuring and interpreting the inherent optical properties. A method is presented to analyze diel cycles in particulate beam-attenuation coefficient (c_p) measured at multiple wavelengths. The method is based on fitting observations with a size-structured population and optical model to infer the particle size distribution and physiologically relevant parameters of the cells responsible for the measured diel cycle in c_p. Results show that the information related to size and contained in the spectral data can be exploited to independently estimate growth and loss rates during the day and night. In addition, the model can characterize the population of particles affecting the c_p diel variability. Application of this method to spectral c_p measured at a station in the oligotrophic Mediterranean Sea suggests that most of the observed variations in c_p can be ascribed to a synchronized population of cells with an equivalent spherical diameter between 1 and 4 µm. The inferred carbon biomass of these cells was about 8–13 mg m^{-3} and accounted for approximately 20% of the total particulate organic carbon. If successfully validated and implemented on autonomous platforms, this method could improve our understanding of the ocean carbon cycle.

1 Introduction

The Earth's climate is profoundly influenced by the ocean biological pump, which absorbs CO_2 from the atmosphere and transfers it to the deep ocean in particulate and dissolved form. Despite its importance, in-situ information on this process is scarce and hard to obtain. Ocean particle dynamics can, however, be investigated by means of the inherent optical properties, which have strong potential to improve understanding of the biological pump.

BGD
8, 3009–3050, 2011

The ocean carbon cycle is also dependent on the Earth's rotation. Indeed, the alternation between day and night imposes a fundamental cycle on photosynthesis and the resulting conversion of atmospheric CO_2 into particulate carbon. As a consequence, diel cycles of bio-geochemical (Burney et al., 1982; Gasol et al., 1998) and optical (Siegel et al., 1989; Cullen et al., 1992; Marra, 1997) properties have been observed in the sunlit ocean.

The particulate beam-attenuation coefficient, c_p, is an inherent optical property that exhibits diurnal variations (e.g., Siegel et al., 1989; Claustre et al., 1999). c_p depends, theoretically, on all the particles present in the water column (i.e., autotrophic and heterotrophic micro-organisms, as well as detritus). In practice however, c_p is mostly influenced by particles with equivalent spherical diameters (ESD) between 0.5 and 20 µm (Pak et al., 1988). Within this size range, each particle pool is expected to contribute a variable fraction of c_p, depending on its number concentration, size, refractive index and shape (e.g., Stramski and Kiefer, 1991). c_p is therefore well correlated with particulate organic carbon concentration (POC), but it has been difficult to ascribe variations of c_p to any specific particle pool, except when additional measurements are available.

Diel variations of particulate beam-attenuation coefficient are widespread in the surface ocean and have long been investigated as a non-invasive tool for deriving particle growth rates and productivity in-situ (Siegel et al., 1989; Cullen et al., 1992; Stramska and Dickey, 1992; Walsh et al., 1995; DuRand and Olson, 1996; Claustre et al., 1999, 2008; Oubelkheir and Sciandra, 2008; Gernez et al., 2011). The diel cycle of c_p is generally characterized by an increase during daytime hours and a decrease at night suggesting that photosynthetic production of particles causes the observed c_p diel cycles (Siegel et al., 1989). These estimates are however considered to be *net* values, because it is assumed that c_p tracks particle concentration, which, in turn, depends on both growth and losses (e.g. Siegel et al., 1989).

Laboratory investigations on phytoplankton cultures have provided significant insights on what controls diel cycles in c_p. First, acclimated pico-phytoplankton (< 2 µm) populations are characterized by remarkably synchronized growth cycles, with division

BGD
8, 3009–3050, 2011

occurring mostly at night, despite the large genetic diversity of this group (Jacquet et al., 2001). Cell cycle synchronization to light availability has also been observed in larger organisms, such as diatoms (Vaulot et al., 1986). Second, diel variations in c_p are more correlated to changes in scattering cross-section (σ_b, a measure of the light scattered by a single cell), than to changes in cell concentration (Stramski and Reynolds, 1993; Stramski et al., 1995; DuRand et al., 2002) and σ_b appears to vary mostly with changes in cell size (DuRand et al. 2002; DuRand and Olson 1998, but see Stramski and Reynolds, 1993).

Flow cytometric analyses of in-situ samples have confirmed and expanded laboratory results. Phytoplankton grow synchronously (i.e., grow during daylight and start dividing around dusk) in different ocean regions (DuRand, 1995; Vaulot and Marie, 1999; Jacquet et al., 2002; Binder and DuRand, 2002) and most of the diel *variations* in c_p can be ascribed to variations in the scattering properties of phytoplankton cells (DuRand, 1995; DuRand and Olson, 1996). Phytoplankton, however, seem to contribute only a fraction of the total c_p (DuRand and Olson, 1996; Claustre et al., 1999; Grob et al., 2007).

Most studies conducted on c_p diel cycles so far employed measurements at a single wavelength (typically 660 nm). The particulate beam attenuation coefficient is, however, wavelength-dependent and its spectral shape can be approximated as a power law (e.g., Boss et al., 2001):

$$c_p(\lambda) = c_p(\lambda_0)\left(\frac{\lambda}{\lambda_0}\right)^{-\gamma}, \quad (1)$$

where $c_p(\lambda_0)$ is c_p at a reference wavelength λ_0 and γ is the spectral slope of c_p.

Interestingly, γ is a proxy for the "average particle size". If the particle size distribution (PSD) can be represented by a power law that spans all possible sizes and with slope ξ, then theoretical (Morel, 1973) and experimental studies (Boss et al., 2001) have shown that the spectral slope of c_p and the slope of the PSD are approximately related according to $\gamma \simeq \xi - 3$ (see also improved relationship presented by Boss et al.,

BGD
8, 3009–3050, 2011

2001). Nevertheless, the practical meaning of "average particle size" remains unclear. Similarly, it is uncertain how the spectral shape of c_p changes when deviations from the PSD power law model occur.

While diel cycles in c_p are well known, cycles in γ have only recently been reported in the open ocean. Two studies showed that γ decreased during the day and increased at night (Oubelkheir and Sciandra, 2008; Slade et al., 2010) suggesting that the relative size of the particles affecting c_p increased during the day and decreased at night. Laboratory studies have also shown diel variability in γ (Claustre et al., 2002; DuRand et al., 2002; Stramski and Reynolds, 1993; Stramski et al., 1995), but only DuRand et al. (2002) clearly reported that γ decreased during the day and increased at night as recently observed in field c_p data.

No attempt has so far been made to exploit the observed variations in γ. We reasoned that it should be possible to estimate *gross* growth rates by measuring diel changes in cell size, because the increase in cell volume during the day should be strictly a result of photosynthetic growth in synchronized cell populations (e.g., Sosik et al., 2003). The objective of the current study was thus to develop a methodology to quantitatively interpret the diel variations in spectral c_p. Specifically, an existing mathematical model was adapted for simulating the diel variations in size and optical properties of a synchronous population of cells. This model was then fitted to in-situ measurements of spectral c_p to infer physiological parameters of this population.

2 Methods

The data analyzed in this study were collected during the early summer of 2008 in the framework of the "Biogeochemistry from the Oligotrophic to the Ultra-oligotrophic Mediterranean" (BOUM) cruise. Specifically, we report on measurements collected during a three-day intensive sampling station that took place in the center of a gyre located in the Algero-Provencal basin (approximately at 39° N and 7° E; Moutin et al., 2011). Water samples were collected continuously from a custom-made clean

BGD
8, 3009–3050, 2011

underway system including a Teflon diaphragm pump to draw water from just under the ship's hull (about 9 m). The average chlorophyll and POC concentrations during this long duration station were approximately 0.05 mg m^{-3} and 50 mg m^{-3}, respectively (Pujo-Pay et al., 2010). Because of the large computational cost of the optimization procedure described below, the inversion scheme was tested on a single day of measurements during which cloud cover was almost absent, as verified by incident PAR measurements.

2.1 In-situ optical measurements

Continuous c_p measurements were collected by a WetLabs ACs hyperspectral absorption and attenuation meter and by two WetLabs C-star transmissometers (nominally centered at 532 and 660 nm). Data were processed following protocols described elsewhere (Dall'Olmo et al., 2009; Slade et al., 2010). All instruments had 25-cm pathlengths. The suitability of the pumping system for conducting these measurements was verified by comparing C-star based $c_p(660)$ values measured on the flow-through system with surface (average between 5 and 15 m) c_p values derived from another C-star transmissometer (nominally, 660 nm, 25-cm pathlength) that was mounted on the CTD. CTD values of c_p were derived by subtracting the minimum c_p value measured at each station from the upcast profiles. This comparison yielded a mean value for the ratio $c_p^{flow} : c_p^{CTD}$ of 0.998 and a standard deviation of 0.071 ($N = 42$). Photosynthetically active radiation (PAR) was determined with a calibrated LI-COR Li-190 quantum sensor mounted on the front mast of the ship.

2.2 Flow cytometric measurements

2 ml samples were collected every hour in cryo-vials from the pump-system described above, fixed using 1% (final) formaldehyde, flash frozen in liquid nitrogen and preserved at −80° C (Troussellier et al., 1995). Samples were later thawed at room temperature and analyzed with a FACSCan flow Cytometer (BD-Biosciences), equipped with an

BGD
8, 3009–3050, 2011

air-cooled argon laser (488 nm, 15 mW). Phytoplanktonic cells were enumerated according to right-angle light scatter properties (SSC, roughly related to cell size), and the orange (585/42 nm) and red (> 650 nm) fluorescence emissions from phycoerythrin and chlorophyll pigments, respectively. 1 µm beads (Polysciences) were added to all samples as internal standard. Data were acquired through the CellQuest software (BD-Biosciences). Four cell types were determined: "Syn", for Synechococcus sp., "euk" for small eukaryotes, and two nanoplankton groups ("nano-1" and "nano-2") according to their increasing SSC and red fluorescence properties. Approximate size ranges for the eukaryotic groups are 1–3 µm for "euk", 3–5 µm for "nano-1" and 5–8 µm for "nano-2". Bacterial counts were obtained on the same sample, after SyBRGreen-I staining (Marie et al., 1997) allowing measurements of their side scattering and green fluorescence (530/30 nm).

2.3 Size-dependent model of cell growth

A discrete time- and size-structured model of cell growth was adapted for the purpose of this study (Gage et al., 1984; Smith, 1996; Arino et al., 2002). The details of the model are reported in the given references, but we describe briefly its main characteristics and the modifications implemented.

The model simulates the biovolume dynamics of a population of phytoplankton cells that is divided into r discrete classes each with a given average size. The cell classes are further divided into two sub-categories: "new born" and "mature". The number of classes for these two categories are r_b and r_d, respectively. "New born" cells are generated from "mature" cells by division and can only grow in size. "Mature" cells grow in size and can also divide according to a given probability, DI. All cells are subject to a generalized loss rate L (see Table 1 for parameter definitions and units).

The cell cycle is subdivided into "growth" and "division" phases occurring during the illuminated and dark parts of the 24-h cycle, respectively. During the growth phase (i.e., the illuminated part of the day), cells can grow exponentially, but do not divide, as supported by the experimental data described above (Fig. 1). During the division

BGD
8, 3009–3050, 2011

phase (i.e., night), cells are only allowed to divide (Fig. 2). Cell loss (e.g., grazing, mixing, cell lysis, etc.) is assumed to be constant, but with different rates between the two phases. The division phase was defined by the times when the values of $c_p(690)$ changed trend and, in practice, corresponded to the part of the 24-h period during which PAR was approximately smaller than 70 µmoles m^{-2} s^{-1}.

Since modeled cells grow exponentially in discrete time steps, the number of size classes is dependent on the cell growth rate and the length of the model iteration (Arino et al., 2002). Here, the iteration period was fixed to 30 min, the maximum growth rate was set to 1 day^{-1} and the resulting total number of classes was 64. These classes were equally sub-divided between "new born" and "mature" cells. Although the number of size classes is known, the average diameter of each size class is determined by the model parameters and cannot be specified a priori. Growth rate, g, was assumed to be light-saturated and uniform among size classes during the growth phase.

The model is formally expressed by the following system of difference equations:

$$\boldsymbol{v}_{t+1} = (1 - L_i)\mathbf{A}_i \boldsymbol{v}_t, \quad (2)$$

where $\boldsymbol{v}_t$ is the vector with the biovolume of each class at time t, L_i is the loss rate, i is the index that distinguishes between day and night and $\mathbf{A}_i$ is the projection matrix. The growth and division expressions for $\mathbf{A}$ are presented in Eqs. (3) and (4) for a simplified case (i.e., $r_b = r_d = 3$):

$$\mathbf{A}_{\text{grow}} = \begin{pmatrix} 1-P & 0 & 0 & 0 & 0 & 0 \\ \text{MP} & 1-P & 0 & 0 & 0 & 0 \\ 0 & \text{MP} & 1-P & 0 & 0 & 0 \\ 0 & 0 & \text{MP} & 1-P & 0 & 0 \\ 0 & 0 & 0 & \text{MP} & 1-P & 0 \\ 0 & 0 & 0 & 0 & \text{MP} & 1 \end{pmatrix} \quad (3)$$

BGD
8, 3009–3050, 2011

$$\mathbf{A}_{\mathrm{div}} = \begin{pmatrix} 1 & 0 & 0 & \mathrm{DI}_1 & 0 & 0 \\ 0 & 1 & 0 & 0 & \mathrm{DI}_2 & 0 \\ 0 & 0 & 1 & 0 & 0 & \mathrm{DI}_3 \\ 0 & 0 & 0 & 1-\mathrm{DI}_1 & 0 & 0 \\ 0 & 0 & 0 & 0 & 1-\mathrm{DI}_2 & 0 \\ 0 & 0 & 0 & 0 & 0 & 1-\mathrm{DI}_3 \end{pmatrix} \quad (4)$$

Here $P = g/(M-1)$ is the fraction of biomass in a given class that grows enough to pass to the next class; and $M = 2^{\frac{1}{r_b+1}}$ is the volume increment for a cell moving from class k to class $k+1$ (for more details see Arino et al., 2002). DI is the fraction of mature cells that is dividing and was assumed to be a linear function of class number:

$$\mathrm{DI}_j = \frac{j}{r_d} p_{\mathrm{DI}}; \quad j = 1, \ldots, r_d \quad (5)$$

where p_{DI} is the maximum value of DI and j is the class index for mature cells.

Each row j of the matrices $\mathbf{A}_{\mathrm{grow}}$ and $\mathbf{A}_{\mathrm{div}}$ represents the interaction of the size class j with the other classes. For example, the third row in $\mathbf{A}_{\mathrm{grow}}$ informs us that, during the illuminated part of the day, the total biovolume of cells belonging to class 3 that is not lost increases due to the growth of cells in class 2 (the MP term in the second column, third row of $\mathbf{A}_{\mathrm{grow}}$) and decreases because part of the biovolume of class 3 grows enough to pass to class 4 (the $1-P$ term in the third column, third row of $\mathbf{A}_{\mathrm{grow}}$). Similarly, the biovolume of class 4 in $\mathbf{A}_{\mathrm{div}}$ that is not lost during a given model iteration decreases due to division (the $1-\mathrm{DI}_1$ term in the fourth column, fourth row of $\mathbf{A}_{\mathrm{div}}$) and, as a consequence, the biovolume of class 1 in $\mathbf{A}_{\mathrm{div}}$ increases (the DI_1 term in the fourth column, first row of $\mathbf{A}_{\mathrm{div}}$).

The solution of Eq. (2) is the distribution of biovolumes in each size class as a function of time. This distribution is then converted into a number distribution (see below) and used to simulate the optical properties of the cell population.

BGD
8, 3009–3050, 2011

2.4 Simulation of optical properties

The particulate beam-attenuation coefficient was assumed to be composed of two spectrally dependent parts: a background component, $c_{p0}(\lambda)$, that was constant throughout the simulation and a time-varying component dependent on the dynamics of the cell population. The cell concentration of each class, N_i, was computed by dividing the biovolume in each class by its mean cellular volume $v_i = M^{k-1} v_{min}$, where $v_{min} = \pi/6 D_{min}^3$ (i.e., cells are assumed to be spherical; Arino et al., 2002). The refractive index of the cell population relative to that of seawater (n) was assumed to be a real number (i.e., absorption was neglected) and constant (in practice the values 1.02, 1.05 and 1.08 were used).

The spectral efficiency factors for attenuation for each class, $Q_{c,i}(\lambda)$, were computed using a standard Mie code (Bohren and Huffman, 1983), accounting for the acceptance angle of the ACs transmissometer (i.e., $\vartheta_0 = 0.93$ degrees):

$$Q_{c,i}(\lambda) = 2\pi \int_{\vartheta_0}^{\pi} \beta_i \sin\vartheta d\vartheta \quad (6)$$

where i is the size-class index, β_i is the volume scattering function for a given size class and ϑ is the scattering angle.

The spectral beam-attenuation coefficient of the population of cells undergoing diel cycles, $c_{pd}(\lambda)$ (the subscript "d" is for "diel"), and for the background, c_{p0}, were then computed as:

$$c_{pd}(\lambda) = \frac{\pi}{4} \sum_{i=1}^{r} N_i D_i^2 Q_{c,i}(\lambda), \quad (7)$$

$$c_{p0}(\lambda) = c_{p0}(500) \left(\frac{\lambda}{500} \right)^{-\gamma_0}. \quad (8)$$

Both $c_{p0}(500)$ and γ_0 are optimization parameters (see below).

BGD
8, 3009–3050, 2011

Finally, the simulated spectral particulate beam-attenuation coefficient was computed as the sum

$$c_p(\lambda) = c_{p0}(\lambda) + c_{pd}(\lambda). \quad (9)$$

2.5 Model inversion

The solutions to Eqs. (2) and (9) were used to simulate a time series of c_p values that was compared to in-situ observations. To obtain a model solution, first the system (Eq. 2) was brought to steady state (the system was solved for 100 iterations, i.e., about 3 months). The resulting biovolume distribution was normalized by the biovolume of class r_b and multiplied by the parameter v_{rb0} to obtain the initial conditions for the following simulation. The system was then solved at each iteration for the entire period and the time-varying spectral c_p was computed.

The model parameters were estimated by minimizing a cost function designed to exploit both the spectral information and the absolute magnitudes of c_p:

$$O = \sum_\lambda \sum_t \left| c_p^{mod}(\lambda,t) - c_p^{obs}(\lambda,t) \right|, \quad (10)$$

where λ was uniformly distributed between 550 and 710 nm with 40 nm intervals. This specific wavelength range was selected to minimize the effects of absorption.

The global optimization algorithm Adaptive Simulated Annealing (http://www.ingber.com/ASA-README.html) was employed to derive robust estimates of the model parameters, which were constrained within realistic ranges (see Table 1). To better constrain the fit at the extremes of the simulation period, the data set used for the fit was composed of one day of data repeated twice and in succession. Thus, the data to be fitted consisted of two identical days of data. To improve the ability of the cost function to detect the global minimum, simulated c_p values were compared to data smoothed by a median filter (window size of 2 h). As traditional simulated annealing, the ASA algorithm introduces random variations in the search for the global optimum and is rather insensitive to initial values of the parameters, given enough time for the optimization.

BGD
8, 3009–3050, 2011

Nevertheless, to test the robustness of our results, the initial values of the parameters were selected randomly from uniformly distributed ranges (Table 1). In addition, the optimization was repeated multiple times for different values of the initial parameters and random seeds. The optimal parameter distributions obtained (see Appendix for details) were used to estimate confidence intervals.

2.6 Carbon estimates

The size distribution of phytoplankton cells retrieved by the inversion scheme affords us with the ability to estimate the carbon biomass, C_ϕ, of the population of cells that drives the diel c_p cycle. Two methods were adopted.

First, the biovolume distribution was converted into phytoplankton carbon by means of published relationships between biovolume and carbon (Montagnes et al., 1994; Menden-Deuer and Lessard, 2000). Of these two studies, the former is considered more relevant to the oligotrophic conditions sampled in the current study, because it was based on data from cells ranging in ESD down to about 2 µm. In contrast, the relationship presented by Menden-Deuer and Lessard (2000) focuses mostly on larger cells (minimum ESD about 7 µm) and thus its application here depends on the conserved nature of the carbon-density vs. biovolume relationship found for large cells.

The second method employed to compute C_ϕ is based on the linear correlation between the real part of the relative refractive index, n, and the intracellular carbon concentration, c_i (Stramski, 1999), which has been confirmed for a variety of species spanning from small cyanobacteria to larger eukaryotes (DuRand et al., 2002): $c_i = 3946\, n - 3922$, where c_i is expressed in kg m^{-3}. Phytoplankton carbon was computed as the product of the estimated biovolume distribution and c_i.

Flow cytometry data were used for preliminary validation of the inverted C_ϕ estimates. Specifically, the carbon biomass of different populations was computed from published values of carbon densities, assumed ranges of cell diameters and measured cellular abundances. Different values were adopted for eukaryotes (0.22 pgC µm^{-3};

BGD
8, 3009–3050, 2011

Booth, 1988) and prokaryotes (0.35 pgC μm^{-3}; Bjornsen, 1986). For comparison, the carbon biomass of heterotrophic bacteria was also estimated.

3 Results

Surface flow cytometric cell abundances did not show clear diel patterns during the course of the long duration station (Fig. 3, left column). On the other hand, diel fluctuations in relative side scattering were evident with increasing values during the day and opposite patterns at night (Fig. 3, right column). Scattering cycles were most clear for the Synechococcus population, but the eukaryote populations ("euk", "nano-1" and perhaps even "nano-2") displayed similar fluctuations, although with larger noise. It is important to note that this larger noise can be related to the wider ranges of cell sizes typical of these populations, rather than to the absence of diel variability. Heterotrophic bacteria did not show clear diel patterns. These diel patters are typical in oceanic regions (e.g., Vaulot and Marie, 1999) and have been previously observed in the surface Mediterranean Sea (Jacquet et al., 2002; Oubelkheir and Sciandra, 2008).

Measured c_p displayed a typical diel cycle, increasing during the day and decreasing at night (Fig. 4). Quantitative spectral differences were however evident: the peak-to-peak variations of $c_p(550)$ were smaller than those of $c_p(690)$ and the maximum value of $c_p(550)$ was broader and lasted about three hours longer than that at $c_p(690)$.

Modeled c_p values were in agreement with measured c_p with median relative residuals ($c_p^{mod}/c_p^{obs} - 1$) spanning from −2% to +3% (Fig. 4). Estimates of model parameters for three different values of the refractive index are presented in Table 2. The relative uncertainties of the parameters were typically below 33%. Most parameters were independent of the refractive index, which suggests that they can be estimated accurately, provided the model assumptions are correct. D_{min} and v_{rd0} were inversely related to n and so were the population time- and size-average diameter and total number of cells (Table 3), suggesting that their individual estimates cannot be considered reliable.

BGD
8, 3009–3050, 2011

Cellular gross growth rate (g) was moderate, amounting to nearly a doubling every two days (Table 2). Cell losses were negligible during the day, but high at night and compensated daytime growth. These results are consistent with previous studies which indicated moderate to high growth rates in oligotrophic regions and near balance between day growth and night losses (Siegel et al., 1989; Lessard and Murrell, 1998; Claustre et al., 2008). The background value of c_p contributed a significant fraction of the measured c_p (~60% at 500 nm), in agreement with the conclusions of other studies (e.g., DuRand and Olson, 1996; Claustre et al., 1999).

Figure 5 presents the size distribution of the cell population as a function of time for the median set of parameters and $n = 1.05$. The cell population gradually increased in size during the illuminated part of the day as a consequence of photosynthetic growth. At dusk (20:24) the population was characterized by a relatively larger number of dividing cells (red empty circles in Fig. 5). As night started, cells divided, new born cells increased in number and the average size of the population decreased. These dynamics are further demonstrated in Fig. 6, where the total number and the average scattering cross-section of cells are plotted. From this figure it is evident that the model ascribes the observed increase in c_p during the illuminated part of the day to an increase in cellular scattering, rather than cell abundance (compare Fig. 6a and b), as suggested by previous studies (e.g., Stramski et al., 1995; DuRand et al., 2002). The c_p dynamics at night are instead related to both variations in cell abundance and scattering cross-section (Fig. 6).

In general, our results are in qualitative agreement with flow cytometry studies that show increases in cell size from dawn to dusk and opposite patterns at night, with negligible changes in cell abundances (Vaulot and Marie, 1999; Jacquet et al., 2002). The specific shape of the modeled size distribution, however, is slightly different from those of observed phytoplankton distributions which are typically log-normal (e.g., Fig. 2a in Stramski et al., 1995 or Fig. 4 in Sosik et al., 2003). This difference is likely caused by the simplified model formulation (e.g., it may require a more complex DI function or implementation of asymmetric cell division). In addition, σ_b decreases faster than

BGD
8, 3009–3050, 2011

flow-cytometric side scattering (compare right column of Figs. 3 and 6b), which is likely related to the assumed function describing the probability of division for each mature cell (DI, Eq. 5). Finally, it is worth mentioning that the total number of cells retrieved by the inversion scheme is in agreement with the combined concentrations of nanoplanktonic cells determined by flow cytometry (compare Figs. 6a and 3).

Phytoplankton carbon estimates based on flow cytometric cell abundances were characterized by large uncertainties due to uncertainties in cell size and carbon densities (Table 4). Nonetheless, nano-eukaryotes ("nano-2" and "nano-1") contributed the majority of the phytoplankton carbon, while pico-eukaryotes ("euk") and Synechococcus ("syn") contributed a considerably smaller fraction of C_{ϕ}. Depending on the parametrization, C_{ϕ} contributed from 5 to 48% of the measured POC (i.e., 50 mg m^{-3}, Pujo-Pay et al., 2010).

The model inferred phytoplankton carbon biomass, C_{ϕ}^{n}, varied by about 37% when n was employed in the calculation and accounted for about 16–26% of the observed POC (Table 5). Instead, variations of up to a factor 5 in the inferred C_{ϕ} were observed when only the PSD and published carbon densities were employed in the calculation, due to the observed covariation between n and $\bar{D}_{\mathrm{avg}}$.

The inversion scheme retrieves C_{ϕ}^{n} of a phytoplankton population distributed over a limited range of diameters (about factor 1.5 between minimum and maximum values, Fig. 5) and likely underestimates the total C_{ϕ}. Thus, the inferred relative contribution of C_{ϕ}^{n} to POC is not inconsistent with previous estimates indicating that the C_{ϕ}:POC ratio is typically around 20–40% in the upper oligotrophic ocean (e.g. DuRand et al., 2001).

4 Discussion

4.1 Partitioning c_{p}

It has long been recognized that the background component of c_{p} can cause significant underestimation of growth rates calculated from diel cycles of c_{p} (e.g., Siegel

BGD
8, 3009–3050, 2011

et al., 1989; Cullen et al., 1992). Here, a simple model was developed that partitions the measured c_p into background and time-varying components. In doing so, the model infers the size distribution of the cell population that is responsible for the diel variations in c_p, as well as other eco-physiological parameters. This is important because the estimated physiological rates are no longer dependent on the background c_p value and the population of particles that most likely affects c_{pd} can now be (partially) characterized.

Some of the model parameters (D_{min} and v_{rb0}), however, were found to be correlated with the refractive index, suggesting that their estimates are unreliable. The correlation between n and D_{min} (or, in general, D) is expected, because these variables appear as a product in the expression for the phase shift parameter ρ that approximately controls Q_c (van de Hulst, 1957). Thus, $(n-1)D$ is a first independent model parameter. On the other hand, D_{min} and v_{rb0} (and similarly $\bar{D}_{avg}$ and $\bar{N}_{tot}$) are inversely related because c_{pd} can be safely approximated as $c_{pd} \approx \bar{N}_{tot}\bar{G}\bar{Q}_c \propto (\bar{N}_{tot}\bar{D}^2)\bar{Q}_c$, since the size distribution of the population that generates the diel component of c_p is rather narrow (van de Hulst, 1957). $\bar{N}_{tot}\bar{D}^2$, is thus a second parameter that partially overlaps with $(n-1)D$.

4.2 Growth and loss rate estimates

The g estimates presented in Table 2 are gross growth rates (i.e. independent of losses). This is a novelty of our model, because previous analyses of c_p diel cycles could only derive net growth rates. The ability of the model to decompose the spectral optical measurements and simultaneously follow biovolume and cell size is the reason why growth and losses can be independently differentiated. Indeed, while biovolume depends both on growth and losses, the average population cell size should be independent of losses, provided that these are not size specific. Consider the average cellular volume at a given time, t:

$$\bar{v}(t) = \frac{\sum v_i(t)N_i(t)}{\sum N_i(t)} \quad (11)$$

BGD
8, 3009–3050, 2011

where the sums are over all the size classes. The intrinsic phytoplankton growth rate based on cellular volume, μ_V, can be computed between sunrise, t_1, and sunset, t_2, as:

$$\mu_V = \frac{1}{t_2 - t_1} \log_e \left(\frac{\bar{v}(t_2)}{\bar{v}(t_1)} \right) f_d, \quad (12)$$

where f_d is the illuminated fraction of the day.

The important property of μ_V is that is depends only on the relative distribution of biovolume across the different size classes (Eq. 11) and not on its absolute value. μ_V (and g) can thus be determined independently of L_d, because the model is able to estimate the relative size of the cells.

This method improves previous single-wavelength c_p-based techniques that can only derive net growth grates and assume daytime losses (e.g., Cullen et al., 1992; Claustre et al., 2008). For comparison, the "diurnal rate of variations" (Eq. (6) in Gernez et al., 2011), scaled by f_d and computed from c_p at 450 and 730 nm were 0.07 and 0.14 d^{-1}, respectively, and significantly lower than g (Table 2). Hence, estimates of growth rate based on single-band c_p measurements, beside being significantly underestimated due to the background c_{p0}, are wavelength dependent and should be used with caution.

Reliable loss estimates during the day and night are fundamental for deriving dependable eco-physiological parameters. For example, Cullen et al. (1992) assumed that $L_d = L_n$ (i.e., "light-independent grazing") and concluded that if $c_{p0} \approx 0.7\, c_p$ then their estimate of growth would be too high. Our model suggests that this conclusion could be invalidated by the assumption of constant loss rates during the day and the night. Flow cytometry data do not show large decreases in cell abundances during the day (but see "euk") and thus are consistent with negligible losses during the day. In addition, the available Acoustic Doppler Current Profiler (ADCP) measurements are consistent with the presence near the surface of relatively large organisms (~2 cm) at night and their absence during the day (Fig. 7). Future investigations should nevertheless focus on validating the current inversion scheme by collecting, among others, in-situ measurements of group specific growth rates.

BGD
8, 3009–3050, 2011

4.3 Phytoplankton carbon estimates

Another novel output of our inversion scheme is the estimated C_{ϕ}^{n} which varied approximately between 8–13 mgC m^{-3} for the different values of n used. These estimates can be used to further characterize the cell population responsible for c_{pd}, by computing time- and size-averages of $c_{pd}^{*} = c_{pd} : C_{\phi}^{n}$ and by comparing these averages with the empirical relationship between carbon-normalized c_p and average particle diameter published by DuRand et al. (2002, their Fig. 9). At 670 nm, the mean (st. dev.) c_{pd}^{*} was equal to 2.50(0.09), 3.69(0.08) and 4.03(0.09) m^2 mgC^{-1} for n=1.02, 1.05 and 1.08 respectively, which corresponds to ESD values between approximately 1 and 4 µm (DuRand et al., 2002).

Note however that small values of n correspond to large values of estimated $\bar{D}$ and to small values of c_{pd}^{*}. Small c_{pd}^{*} values should instead coincide with smaller cells (Fig. 9, DuRand et al., 2002). Thus, our model is unable to resolve these differences and attention should be focused on its average results.

From the above analysis, nevertheless, it appears that the phytoplankton responsible for the diel variations of c_p were cells larger than typical cyanobacteria. This range of ESD is not too far from the average $D = 5.2$ µm retrieved for the most typical value of n for phytoplankton (i.e., 1.05; Table 3), is in agreement with the flow cytometry data that showed diel variations in the relative side-scattering of eukaryotic populations (Fig. 1) and is consistent with previous findings suggesting that nano-eukaryotic cells contributed most of c_{pd} (DuRand and Olson, 1996).

4.4 Productivity estimates

Net diurnal productivity was computed from the model output and compared to single-band c_p estimates. The difference in population carbon biomass between dusk and dawn normalized to the time difference yielded a median value of 4.7(0.9) mgC m^{-3} d^{-1} for n varying from 1.02 to 1.08. On the other hand, the rate of POC increase between

BGD
8, 3009–3050, 2011

dusk and dawn was calculated from measurements of $c_p(670)$ and yielded 4.5(0.8) and 3.5(0.6) mgC m^{-3} d^{-1}, for a conversion factor between POC and $c_p(670)$ of 2.0 m^2 gC^{-1} (Claustre et al., 1999) and 2.6 m^2 gC^{-1} (Gardner et al., 2006), respectively.

The c_p^* values typically adopted to compute productivity from c_p cycles are derived empirically using *bulk* c_p and POC measurements. These c_p^* are therefore dependent on the background components of both POC and c_p and assume that the same carbon-to-attenuation ratios exist for background and time-varying components of the particle pool. The relatively small differences found between the resulting productivity estimates and those derived from our model suggest that conversion factors were similar for c_{pd} and c_{p0} in the current study.

For comparison, particulate primary production estimates based on ^{14}C additions amounted to approximately 2.5 mgC m^{-3} d^{-1} (López-Sandoval et al., 2010) and were thus significantly lower than those estimated using the in-situ c_p values. This mismatch with estimates based on incubation techniques has been observed in the past (Claustre et al., 2008; Quay et al., 2010) and our data add to the building evidence suggesting that bottle artifacts may be introducing biases in productivity estimates.

4.5 Limitations

An important limitation of the current technique is its large computational cost. Despite each set of global optimizations being distributed to several parallel processors, relatively long running times (about 12 h with over 40 CPUs) were required to identify the global optima for each n. Nevertheless, we expect that improved hardware and smarter algorithms will become available, making the current technique (or adaptation thereof) more affordable. Limitations from the eco-physiological and optical point of view are stated in the model assumptions. Important issues include the assumption that only one population of cells is responsible for the observed cycle in c_p and the assumptions of constant growth and loss rates during the two simulated phases of the cell cycle.

BGD
8, 3009–3050, 2011

Modeled and observed c_p values are in agreement, however, it is clear that the fit is not perfect and the largest deviations occur at the transition point between day and night (i.e., when cells start dividing, Fig. 4). Different species are known to start dividing at different times (Vaulot and Marie, 1999; Binder and DuRand, 2002) and assuming a single species is responsible for all of the diel variations in c_p is likely the cause of the mismatch between model and observations. The time-discrete model potentially introduces additional discrepancies especially at the transition between day an night, when the model form changes significantly (see Figs. 1 and 2 and Eqs. 3 and 4). Furthermore, assuming a constant growth rate during the illuminated period may also be questionable as it has been shown that synchronized cells may alter their physiological status depending on the stage of the cell cycle (Harding et al., 1981; Bruyant et al., 2005; Gernez et al., 2011). Finally, it is possible that the time varying population generates a time varying detrital component that is ignored by our model, potentially skewing the interpretation of the inferred eco-physiological and morphological parameters.

Nevertheless, these approximations represented a trade off between model complexity and information content of the data. It is unlikely that more parameters could be estimated from the available c_p data, but inclusion of additional independent pieces of information (e.g., angularly resolved scattering data) may permit greater complexity to be resolved and may yield more robust results.

Future work, however, should first implement and test the method under different environments. One interesting feature that our model was unable to capture, and that may also benefit from further studies, is the specific relationship between carbon-normalized c_p and n (Fig. 9, DuRand et al., 2002).

5 Conclusions

A model was developed to invert measurements of spectral particulate beam attenuation collected over a diel cycle. The model partitions c_p into constant and time-varying components and outputs novel, independent estimates of growth and loss rates, as

BGD
8, 3009–3050, 2011

well as the carbon biomass of the population of cells responsible for the measured variability in c_p.

This technique is considerably different from previous work based on measurements at a single wavelength. Specifically, no assumptions are made regarding the background component of c_p and the carbon-to-c_p conversion factor. The derived gross growth and net diurnal productivity rates can be, as a consequence, significantly different from those estimated from single-band c_p cycles.

The method presented retains the appeal of previous work on c_p diel cycles as it only requires measurements of particulate beam-attenuation at multiple wavelengths. If successfully validated, it could provide a powerful way to assess the eco-physiological status of phytoplankton populations from measurements collected by autonomous platforms, thus enhancing our understanding of the ocean carbon cycle.

Appendix A

Selection of optimal sets of parameters

As stated in the Methods section, for each value of n several optimizations were run for different initial values of the parameters and random seeds. Despite each optimization required around 10^6 iterations, the global minimum was not always reached. The "solution space" (i.e. all the parameters retrieved by each optimization as a function of the cost function) is presented in Figs. 8–10. The retrieved parameters clustered in certain regions of the solution space. Thus, it became necessary to devise a reproducible methodology to extract the optimal set of parameters and their uncertainties. We proceeded as follows. We focused on the parameter D_{min}, because it produced clear clusters of results and selected the cluster for which the cost function reached the minimum values. We called this set of solutions the "optimal set of parameters". Figures 8–10 present the results of all optimizations as well as the selected optimal sets of parameters.

BGD
8, 3009–3050, 2011

Acknowledgements. The authors would like to thank the captain, chief engineer, electricians and crew of the N/O *L'Atalante* for their support during the cruise. S. Sakatahe is thanked for making available the "asamin" interface (http://faculty.arts.ubc.ca/ssakata/public_html/software/) which was employed to run the ASA algorithm within GNU Octave. S. Bonnet is thanked for providing the Teflon pump used for the pumping system. M. Grant at PML is acknowledged for his help with distributed computing. G.D.O. was supported through NASA grant NNX09AK30G and the UK National Centre for Earth Observations.

References

Arino, J., Gouze, J. L., and Sciandra, A.: A discrete, size-structured model of phytoplankton growth in the chemostat – Introduction of inhomogeneous cell division size, J. Math. Biol., 45, 313–336, doi:10.1007/s002850200160, 2002. 3016, 3017, 3018, 3019

Binder, B. J. and DuRand, M. D.: Diel cycles in surface waters of the equatorial Pacific, Deep-Sea Res. Pt. II, 49, 2601–2617, 2002. 3013, 3029

Bjornsen, P. K.: Automatic-determination of bacterioplankton biomass by image-analysis, Appl. Environ. Microb., 51, 1199–1204, 1986. 3022, 3039

Bohren, C. F. and Huffman, D. R.: Absorption and scattering of light by small particles, Wiley, New York, 1983. 3019

Booth, B. C.: Size classes and major taxonomic groups of phytoplankton at 2 locations in the subarctic Pacific-ocean in May and August, 1984, Mar. Biol., 97, 275–286, 1988. 3022, 3039

Boss, E., Twardowski, M. S., and Herring, S.: Shape of the particulate beam attenuation spectrum and its inversion to obtain the shape of the particulate size distribution, Appl. Optics, 40, 4885–4893, 2001. 3013

Bruyant, F., Babin, M., Genty, B., Prasil, O., Behrenfeld, M. J., Claustre, H., Bricaud, A., Garczarek, L., Holtzendorff, J., Koblizek, M., Dousova, H., and Partensky, F.: Diel variations in the photosynthetic parameters of Prochlorococcus strain PCC 9511: Combined effects of light and cell cycle, Limnol. Oceanogr., 50, 850–863, 2005. 3029

Burney, C. M., Davis, P. G., Johnson, K. M., and Sieburth, J. M.: Diel relationships of microbial trophic groups and in situ dissolved carbohydrate dynamics in the Caribbean sea, Mar. Biol., 67, 311–322, 1982. 3012

Claustre, H., Morel, A., Babin, M., Cailliau, C., Marie, D., Marty, J. C., Tailliez, D., and Vaulot,

BGD

8, 3009–3050, 2011

D.: Variability in particle attenuation and chlorophyll fluorescence in the tropical Pacific: Scales, patterns, and biogeochemical implications, J. Geophys. Res.-Oceans, 104, 3401–3422, 1999. 3012, 3013, 3023, 3028

Claustre, H., Bricaud, A., Babin, M., Bruyant, F., Guillou, L., Le Gall, F., Marie, D., and Partensky, F.: Diel variations in Prochlorococcus optical properties, Limnol. Oceanogr., 47, 1637–1647, 2002. 3014

Claustre, H., Huot, Y., Obernosterer, I., Gentili, B., Tailliez, D., and Lewis, M.: Gross community production and metabolic balance in the South Pacific Gyre, using a non intrusive bio-optical method, Biogeosciences, 5, 463–474, doi:10.5194/bg-5-463-2008, 2008. 3012, 3023, 3026, 3028

Cullen, J. J., Lewis, M. R., Davis, C. O., and Barber, R. T.: Photosynthetic characteristics and estimated growth-rates indicate grazing is the proximate control of primary production in the equatorial pacific, J. Geophys. Res.-Oceans, 97, 639–654, 1992. 3012, 3025, 3026

Dall'Olmo, G., Westberry, T. K., Behrenfeld, M. J., Boss, E., and Slade, W. H.: Significant contribution of large particles to optical backscattering in the open ocean, Biogeosciences, 6, 947–967, doi:10.5194/bg-6-947-2009, 2009. 3015

DuRand, M. D.: Phytoplankton growth and diel variations in beam attenuation through individual cell analysis, Ph.D. thesis, MIT, WHOI, 1995. 3013

DuRand, M. D. and Olson, R. J.: Contributions of phytoplankton light scattering and cell concentration changes to diel variations in beam attenuation in the equatorial Pacific from flow cytometric measurements of pico-, ultra- and nanoplankton, Deep-Sea Res. Pt. II, 43, 891–906, 1996. 3012, 3013, 3023, 3027

DuRand, M. D. and Olson, R. J.: Diel patterns in optical properties of the chlorophyte Nannochloris sp.: Relating individual-cell to bulk measurements, Limnol. Oceanogr., 43, 1107–1118, 1998. 3013

DuRand, M. D., Olson, R. J., and Chisholm, S. W.: Phytoplankton population dynamics at the Bermuda Atlantic Time-series station in the Sargasso Sea, Deep-Sea Res. Pt. II, 48, 1983–2003, 2001. 3024

DuRand, M. D., Green, R. E., Sosik, H. M., and Olson, R. J.: Diel variations in optical properties of Micromonas pusilla (Prasinophyceae), J. Phycol., 38, 1132–1142, 2002. 3013, 3014, 3021, 3023, 3027, 3029

Gage, T. B., Williams, F. M., and Horton, J. B.: Division synchrony and the dynamics of microbial-populations – A size-specific model, Theor. Popul. Biol., 26, 296–314, 1984. 3016

BGD
8, 3009–3050, 2011

Gardner, W. D., Mishonov, A., and Richardson, M. J.: Global POC concentrations from in-situ and satellite data, Deep-Sea Res. Pt. II, 53, 718–740, 2006. 3028
Gasol, J. M., Doval, M. D., Pinhassi, J., Calderon-Paz, J. I., Guixa-Boixareu, N., Vaque, D., and Pedros-Alio, C.: Diel variations in bacterial heterotrophic activity and growth in the northwestern Mediterranean Sea, Mar. Ecol.-Prog. Ser., 164, 107–124, 1998. 3012
Gernez, P., Antoine, D., and Huot, Y.: Diel cycles of the particulate beam attenuation coefficient under varying trophic conditions in the northwestern Mediterranean Sea: Observations and modeling, Limnol. Oceanogr., 56, 17–36, 2011. 3012, 3026, 3029
Grob, C., Ulloa, O., Claustre, H., Huot, Y., Alarcón, G., and Marie, D.: Contribution of picoplankton to the total particulate organic carbon concentration in the eastern South Pacific, Biogeosciences, 4, 837–852, doi:10.5194/bg-4-837-2007, 2007. 3013
Harding, L. W., Prezelin, B. B., Sweeney, B. M., and Cox, J. L.: Diel oscillations in the photosynthesis-irradiance relationship of a planktonic marine diatom, J. Phycol., 17, 389–394, 1981. 3029
Jacquet, S., Partensky, F., Lennon, J. F., and Vaulot, D.: Diel patterns of growth and division in marine picoplankton in culture, J. Phycol., 37, 357–369, 2001. 3013
Jacquet, S., Prieur, L., Avois-Jacquet, C., Lennon, J. F., and Vaulot, D.: Short-timescale variability of picophytoplankton abundance and cellular parameters in surface waters of the Alboran Sea (western Mediterranean), J. Plankton Res., 24, 635–651, 2002. 3013, 3022, 3023
Lessard, E. J. and Murrell, M. C.: Microzooplankton herbivory and phytoplankton growth in the northwestern Sargasso Sea, Aquat. Microb. Ecol., 16, 173–188, 1998. 3023
López-Sandoval, D. C., Fernández, A., and Marañón, E.: Dissolved and particulate primary production along a longitudinal gradient in the Mediterranean Sea, Biogeosciences Discuss., 7, 8591–8617, doi:10.5194/bgd-7-8591-2010, 2010. 3028
Marie, D., Partensky, F., Jacquet, S., and Vaulot, D.: Enumeration and cell cycle analysis of natural populations of marine picoplankton by flow cytometry using the nucleic acid stain SYBR Green I, Appl. Environ. Microb., 63, 186–193, 1997. 3016
Marra, J.: Analysis of diel variability in chlorophyll fluorescence, J. Mar. Res., 55, 767–784, 1997. 3012
Menden-Deuer, S. and Lessard, E. J.: Carbon to volume relationships for dinoflagellates, diatoms, and other protist plankton, Limnol. Oceanogr., 45, 569–579, 2000. 3021, 3039, 3040
Montagnes, D. J. S., Berges, J. A., Harrison, P. J., and Taylor, F. J. R.: Estimating carbon, nitrogen, protein, and chlorophyll-a from volume in marine-phytoplankton, Limnol. Oceanogr.,

BGD
8, 3009–3050, 2011

39, 1044–1060, 1994. 3021, 3039, 3040
Morel, A.: Advisory Group for Aerospace Research and Development, chap. Diffusion de la lumiere par les eaux de mer, Resultat experimentaux et approach theorique, NATO, 1–76, 1973. 3013
Moutin, T., Van Wambeke, F., and Prieur, L.: Introduction to the Biogeochemistry from the Oligotrophic to the Ultraoligotrophic Mediterranean (BOUM) experiment, Biogeosciences Discuss., in preparation, 2011. 3014
Oubelkheir, K. and Sciandra, A.: Diel variations in particle stocks in the oligotrophic waters of the Ionian Sea (Mediterranean), J. Marine Syst., 74, 364–371, 2008. 3012, 3014, 3022
Pak, H., Kiefer, D. A., and Kitchen, J. C.: Meridional variations in the concentration of chlorophyll and microparticles in the North Pacific Ocean, Deep-Sea Res., 35, 1151–1171, 1988. 3012
Pujo-Pay, M., Conan, P., Oriol, L., Cornet-Barthaux, V., Falco, C., Ghiglione, J.-F., Goyet, C., Moutin, T., and Prieur, L.: Integrated survey of elemental stoichiometry (C, N, P) from the Western to Eastern Mediterranean Sea, Biogeosciences Discuss., 7, 7315–7358, doi:10.5194/bgd-7-7315-2010, 2010. 3015, 3024
Quay, P. D., Peacock, C., Bjorkman, K., and Karl, D. M.: Measuring primary production rates in the ocean: Enigmatic results between incubation and non-incubation methods at Station ALOHA, Global Biogeochem. Cy., 24, GB3014, doi:10.1029/2009GB003665, 2010. 3028
Siegel, D., Dickey, T., Washburn, L., Hamilton, M., and Mitchell, B.: Optical determination of particulate abundance and production variations in the oligotrophic ocean, Deep-Sea Res., 36, 211–222, 1989. 3012, 3023, 3024
Slade, W. H., Boss, E., Dall'Olmo, G., Langner, M. R., Loftin, J., Behrenfeld, M. J., Roesler, C., and Westberry, T. K.: Underway and moored methods for improving accuracy in measurement of spectral particulate absorption and attenuation, J. Atmos. Ocean. Tech., 27, 1733–1746, 2010. 3014, 3015
Smith, H. L.: A discrete, size-structured model of microbial growth and competition in the chemostat, J. Math. Biol., 34, 734–754, 1996. 3016
Sosik, H. M., Olson, R. J., Neubert, M. G., Shalapyonok, A., and Solow, A. R.: Growth rates of coastal phytoplankton from time-series measurements with a submersible flow cytometer, Limnol. Oceanogr., 48, 1756–1765, 2003. 3014, 3023
Stramska, M. and Dickey, T. D.: Variability of biooptical properties of the upper ocean associated with diel cycles in phytoplankton population, J. Geophys. Res.-Oceans, 97, 17873–17887, 1992. 3012

BGD
8, 3009–3050, 2011

Stramski, D.: Refractive index of planktonic cells as a measure of cellular carbon and chlorophyll a content, Deep-Sea Res. Pt. I, 46, 335–351, 1999. 3021
Stramski, D. and Kiefer, D.: Light scattering by microorganisms in the open ocean, Prog. Oceanogr., 28, 343–383, 1991. 3012
Stramski, D. and Reynolds, R. A.: Diel variations in the optical-properties of a marine diatom, Limnol. Oceanogr., 38, 1347–1364, 1993. 3013, 3014
Stramski, D., Shalapyonok, A., and Reynolds, R. A.: Optical characterization of the oceanic unicellular cyanobacterium Synechococcus grown under a day-night cycle in natural irradiance, J. Geophys. Res.-Oceans, 100, 13295–13307, 1995. 3013, 3014, 3023
Troussellier, M., Courties, C., and Zettelmaier, S.: Flow cytometric analysis of coastal lagoon bacterioplankton and picophytoplankton – Fixation and storage effects, Estuar. Coast. Shelf S., 40, 621–633, 1995. 3015
van de Hulst, H. C.: Light scattering by small particles, Wiley, New York, 1957. 3025
Vaulot, D. and Marie, D.: Diel variability of photosynthetic picoplankton in the equatorial Pacific, J. Geophys. Res.-Oceans, 104, 3297–3310, 1999. 3013, 3022, 3023, 3029
Vaulot, D., Olson, R. J., and Chisholm, S. W.: Light and dark control of the cell cycle in two marine phytoplankton species, Exp. Cell Res., 167, 38–52, 1986. 3013
Vrede, K., Heldal, M., Norland, S., and Bratbak, G.: Elemental composition (C, N, P) and cell volume of exponentially growing and nutrient-limited bacterioplankton, Appl. Environ. Microb., 68, 2965–2971, doi:10.1128/AEM.68.6.2965-2971.2002, 2002. 3039
Walsh, I. D., Chung, S. P., Richardson, M. J., and Gardner, W. D.: The diel cycle in the integrated particle load in the Equatorial Pacific – A comparison with primary production, Deep-Sea Res. Pt. II, 42, 465–477, 1995. 3012

BGD
8, 3009–3050, 2011

Table 1. Definitions, ranges and units of model parameters.

Parameter	Definition	Range min	Range max	Units
L_d	day-time volume-specific loss rate	0	$2/T$	1/iteration
L_n	night-time volume-specific loss rate	0	$2/T$	1/iteration
g	volume-specific growth rate	0	$1/T$	1/iteration
D_{min}	minimum cellular diameter	0.2	20	µm
v_{rb0}	biovolume of class r_b at $t = t_0$	10	10^5	$\mu m^3\,cm^{-3}$
p_{DI}	maximum of DI	0	1	–
$c_{p0}(500)$	background c_p at 500 nm	0	0.09	m^{-1}
γ_0	spectral slope of background c_p	–2	2	–

BGD
8, 3009–3050, 2011

Table 2. Median and central 68th percentile range of estimated model parameters for three different nominal values of n (units as in Table 1 except for g and L_n that are reported in units of day^{-1}). g, L_d and L_n are all scaled by the corresponding fraction of the day.

n	g	L_d	L_n	D_{min}	x_{rb0}	p_{DI}	$c_{p0}(500)$	γ_0
1.02	0.33(0.04)	0.0001(0.0134)	0.32(0.05)	9.6(0.6)	3665(1211)	0.98(0.11)	0.048(0.008)	0.52(0.23)
1.05	0.33(0.03)	0.0010(0.0180)	0.32(0.06)	4.5(0.2)	1101(283)	0.99(0.07)	0.049(0.009)	0.48(0.13)
1.08	0.32(0.04)	0.0002(0.0260)	0.31(0.06)	2.9(0.1)	696(211)	0.96(0.10)	0.047(0.011)	0.52(0.11)

BGD
8, 3009–3050, 2011

Table 3. Median and central 68th percentile range of cell population parameters estimated from model outputs for three different nominal values of n (units as in Table 1). $\bar{D}_{avg}$ and $\bar{N}_{tot}$ are the 24-h averages of D_{avg} and N_{tot}, respectively.

n	$\bar{D}_{avg}$	$\bar{N}_{tot}$
1.02	11.1(0.7)	166 (39)
1.05	5.2(0.2)	498(155)
1.08	3.4(0.1)	1155(439)

BGD
8, 3009–3050, 2011

Table 4. Phytoplankton and heterotrophic bacterial carbon (mg m^{-3}) estimated from flow cytometric cell abundances, equivalent spherical diameters (ESD) and published carbon densities. C_ϕ is the total phytoplankton carbon, C_{HB} is the carbon of heterotrophic bacteria. Different values of carbon density were used: in BB the value for eukaryotes was 0.22 pgC μm^{-3} (Booth, 1988) while that for Synechococcus and heterotrophic bacteria (HB) was 0.35 pgC μm^{-3} (Bjornsen, 1986); in M94 and MDL00 algal carbon densities were taken from the relationships published by Montagnes et al. (1994) and Menden-Deuer and Lessard (2000), respectively. HB carbon density was 0.148 pgC μm^{-3} (exponentially growing organisms, Vrede et al., 2002) in M94 and 0.039 pgC μm^{-3} in MDL00 (phosphorous limited, Vrede et al., 2002).

	Nano2	Nano1	Euk	Syn	HB	C_ϕ	C_ϕ+C_{HB}
ESD (µm)	5–8	3–5	1–3	0.8–1.0	0.4–0.8		
cells ml^{-1}	291(43)	359(50)	205(32)	6123(507)	342 907(41 368)		
BB	4.2–17.2	1.1–5.2	0.0–0.6	0.6–1.1	4.0–32.2	5.9–24.1	9.9–56.3
M94	2.0–8.1	0.5–2.5	0.0–0.3	0.2–0.4	1.7–13.6	2.7–11.3	6.9–39.0
MDL00	3.0–12.4	0.9–4.1	0.0–0.6	0.4–0.7	0.4–3.6	4.3–17.7	4.7–21.3

BGD
8, 3009–3050, 2011

Table 5. Phytoplankton carbon ($mg\,m^{-3}$) inferred from model outputs by means of the biovolume-*n* relationship, C_{ϕ}^{n} and from the model biovolume and the carbon-biovolume relationships by Montagnes et al. (1994), C_{ϕ}^{M94}, and Menden-Deuer and Lessard (2000), C_{ϕ}^{ML00}.

	1.02	1.05	1.08
C_{ϕ}^{n}	13.1(4.0)	8.5(2.0)	8.2(2.2)
C_{ϕ}^{M94}	12.8(3.9)	3.9(0.9)	2.5(0.7)
C_{ϕ}^{ML00}	16.7(4.8)	5.4(1.2)	3.5(0.9)

BGD
8, 3009–3050, 2011

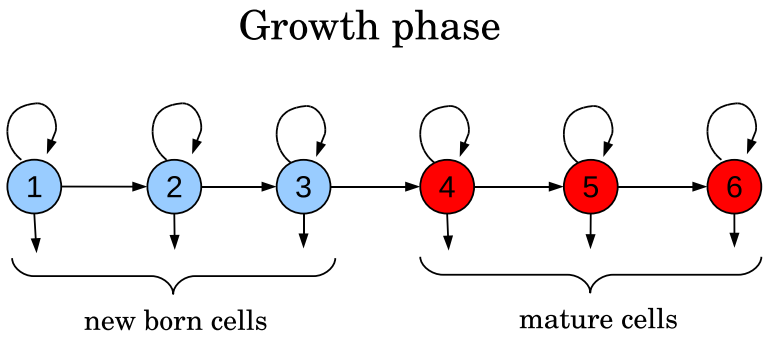

Fig. 1. Schematic representation for the model structure during the growth (illuminated) part of the day, for the specific case in which both the number of new born cells and of mature cells is three. Each circle corresponds to a given size class, with size increasing from class 1 to class 6. Arrows connecting circles represent growth, arrows pointing down represent losses and arrows returning to the same circle represent cells that did not grow enough to pass to the next size class.

BGD
8, 3009–3050, 2011

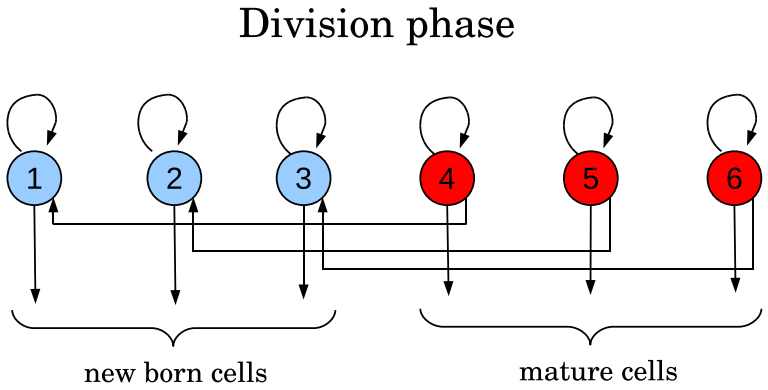

Fig. 2. Schematic representation for the model structure during the division (dark) part of the day, for the specific case in which the number of new born cells and of mature cells is three. Arrows connecting circles represent division, arrows pointing down represent losses and arrows returning to the same circle represent cells that are not dividing.

BGD
8, 3009–3050, 2011

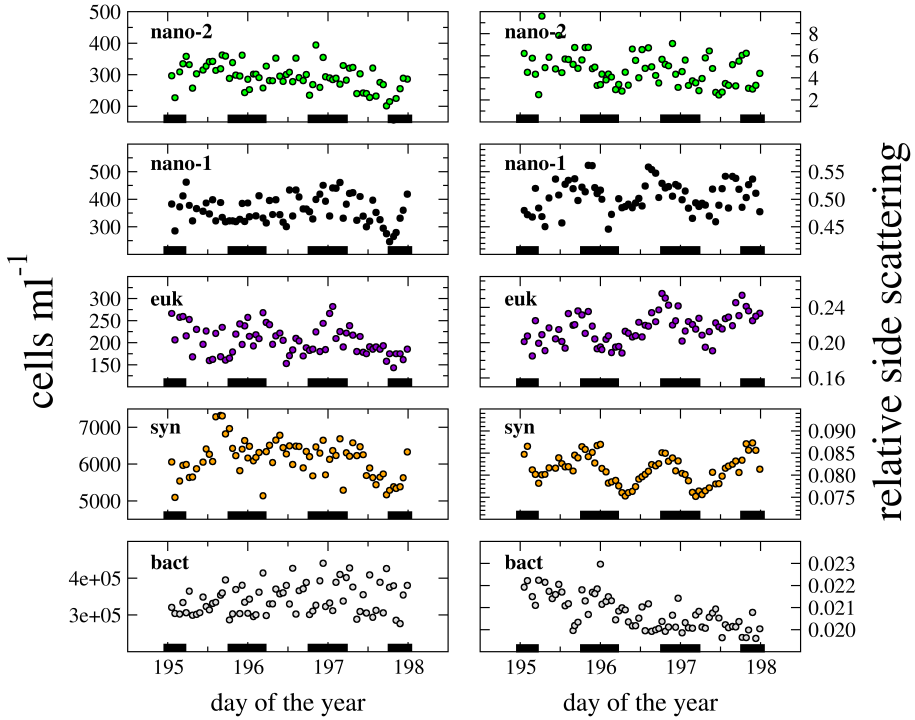

Fig. 3. Time series of flow cytometric estimates of cell abundance (left column) and side scattering relative to 1 µm beads (right column). Black bars on the x-axes indicate the night-time periods. Prochlorococcus was not reliably detected by the instrument used for the analysis.

BGD
8, 3009–3050, 2011

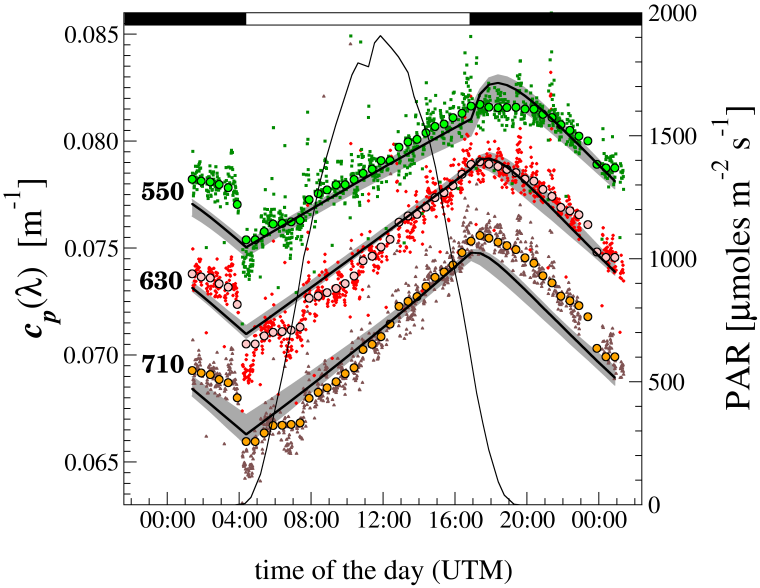

Fig. 4. Comparison between measured and modeled c_p. Time series of c_p measured at different wavelengths (bold numbers) are presented as small colored dots together with their median filtered values used for the optimization (large circles). Gray shaded areas and thinner black lines are the 95% confidence intervals and median, respectively, of modeled c_p at the same wavelengths ($n = 1.05$). The photosynthetically available radiation (PAR) is plotted as the thin bell-shaped black line. Black and white bar at the top indicate the division and growth phases of the model, respectively.

BGD
8, 3009–3050, 2011

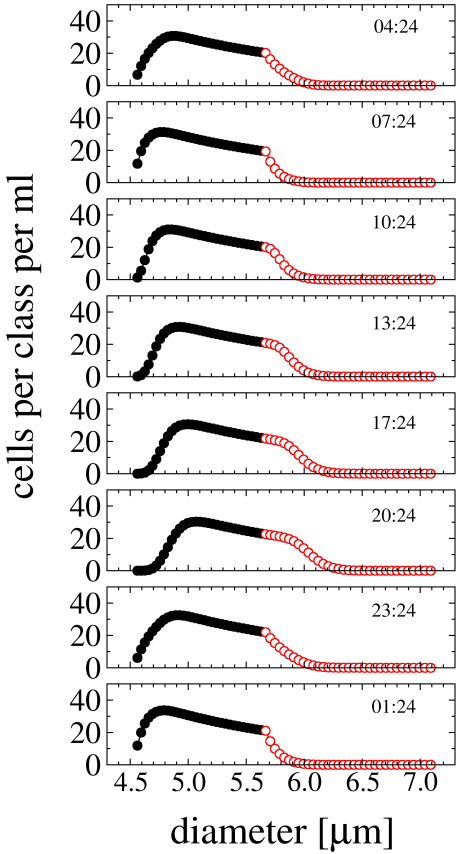

Fig. 5. Model output for cell number concentrations for each class plotted from top to bottom every three hours since day of the year 196.1 (results obtained for the median of the optimal parameters and $n = 1.05$). Black filled circles: newborn cells; red open circles: dividing cells. Daytime hours in this plot start after 07:24 and ends at 20:24.

BGD
8, 3009–3050, 2011

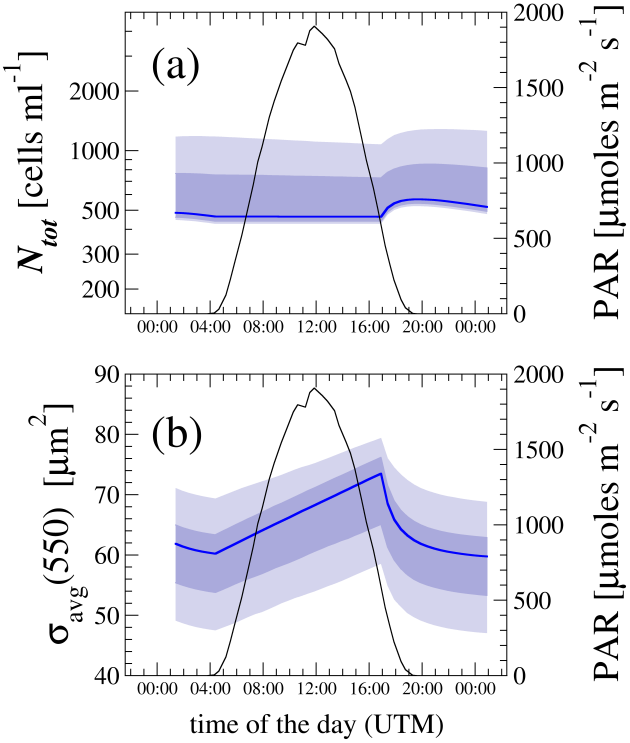

Fig. 6. Inferred total number of cells **(a)** and average population scattering cross-section at 550 nm **(b)** as a function of time ($n = 1.05$). Thick blue lines: median values; dark blue shaded areas: central 68th percentile range (approximately equal to the standard deviation for normal distributions); light blue shaded areas: 95% confidence intervals. The photosynthetically available radiation (PAR) is plotted as a thin black line.

BGD
8, 3009–3050, 2011

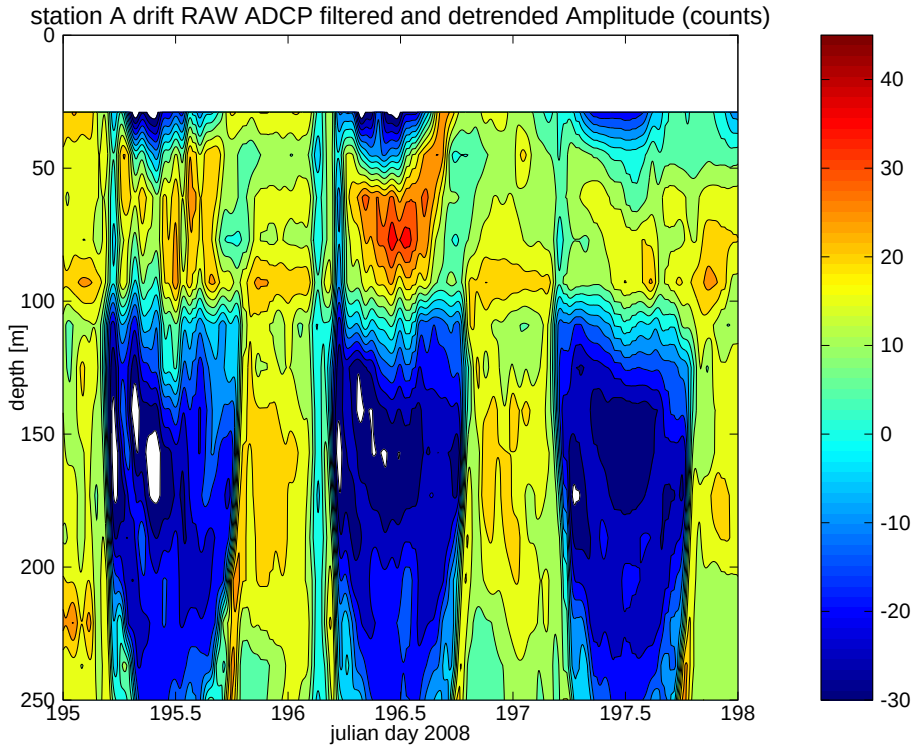

Fig. 7. Time series of vertical profiles of ADCP (78 khz) estimates of raw acoustic backscattering signal filtered (30 min window) and detrended to remove water absorption. The minimum bin depth was about 29 m.

BGD
8, 3009–3050, 2011

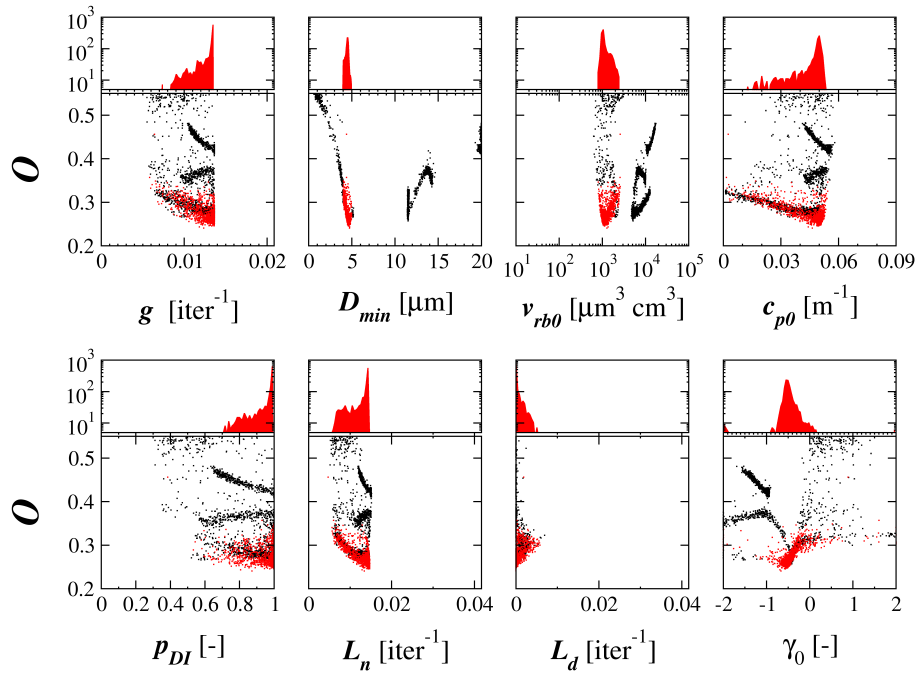

Fig. 8. Results of 4115 optimizations for $n = 1.05$. Values of the cost function O are plotted for each parameter (large plots). Black dots: all results; red dots: optimal parameters (1264 points). Smaller plots show the frequency distribution of the optimal parameters (note logarithmic y-axes). The limits of the x-axes span the the range allowed by the constraints (Table 1). The criterion to select the optimal set of parameters was $3 \leq D_{\min} \leq 5\,\mu m$.

BGD
8, 3009–3050, 2011

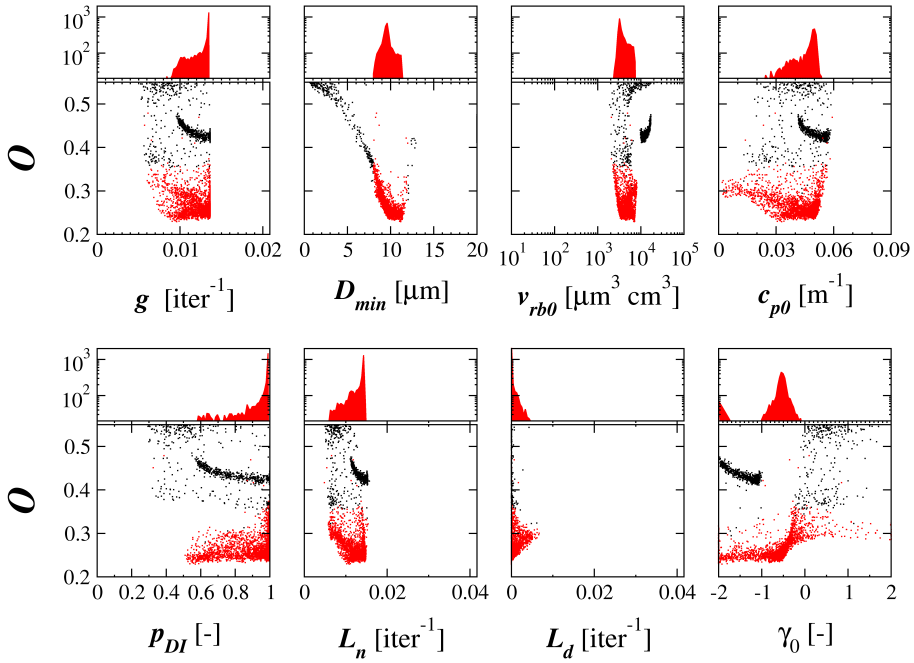

Fig. 9. Results of 4634 optimizations for $n = 1.02$. Values of the cost function O are plotted for each parameter (large plots). Black dots: all results; red dots: optimal parameters (3197 points). Smaller plots show the frequency distribution of the optimal parameters. The limits of the x-axes span the the range allowed by the constraints (Table 1). The criterion to select the optimal set of parameters was $8 \leq D_{min} \leq 12\,\mu m$.

BGD
8, 3009–3050, 2011

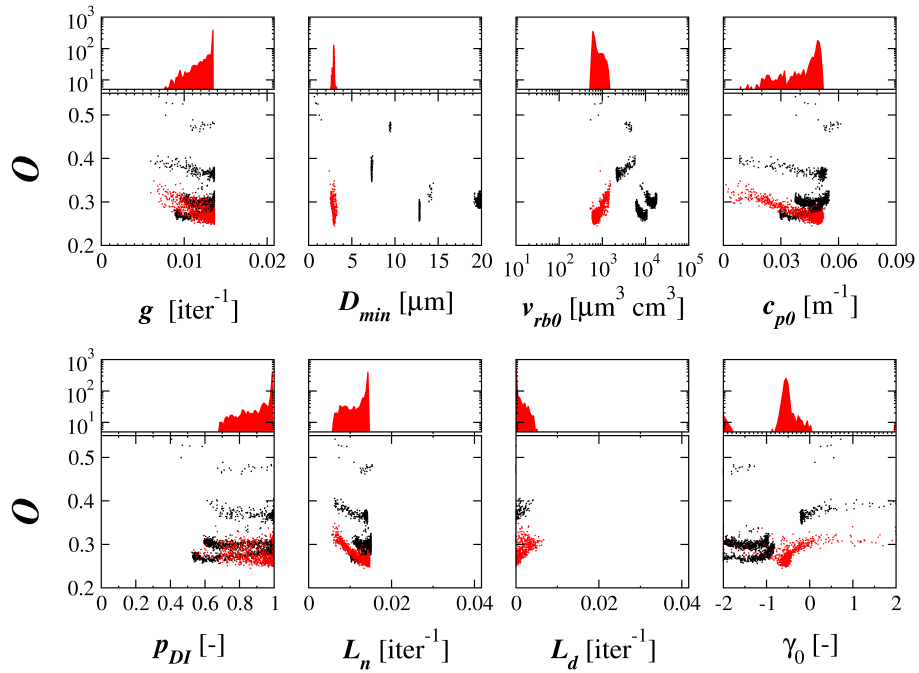

Fig. 10. Results of 3221 optimizations for $n = 1.08$. Values of the cost function O are plotted for each parameter (large plots). Black dots: all results; red dots: optimal parameters (1069 points). Smaller plots show the frequency distribution of the optimal parameters. The limits of the x-axes span the the range allowed by the constraints (Table 1). The criterion to select the optimal set of parameters was $2 \leq D_{min} \leq 4$ µm.

BGD
8, 3009–3050, 2011